RSC Advances

PAPER

View Article Online
View Journal | View Issue

Cite this: *RSC Adv.*, 2025, **15**, 39847

Thermodynamic insights into the interplay between calcium and iron(II) hydroxycarboxylates: impacts on solubility, speciation, and bioavailability

Yi Li,[ab] Yongqiang Cheng [ab] and Ning Tang *[ab]

This study investigated the aqueous solubility, speciation, and thermodynamic properties of calcium and iron(II) hydroxycarboxylates to elucidate their complex interactions and optimize mineral supplement formulations. The results showed that the solubility of these compounds increased with temperature, with calcium lactate exhibiting higher solubility than calcium gluconate, while iron(II) gluconate had higher solubility than iron(II) lactate. The thermodynamic analysis revealed that the dissolution processes were endothermic and entropy-driven. Additionally, the presence of iron(II) ions was found to enhance the solubility of calcium hydroxycarboxylates, likely due to competitive complexation and suppression of ion pairing. In mixed systems containing both calcium and iron(II) hydroxycarboxylates, homologous systems (same anion) exhibited decreased solubilities due to the common ion effect, and the presence of a competing salt significantly altered the dissolution thermodynamics, with the effect being more pronounced for the less soluble salt. While cross-ligand systems (different anions) showed complex dissolution behavior involving rapid one-step and step-wise ion exchange processes, leading to supersaturation and precipitation. Isothermal titration calorimetry provided insights into the thermodynamics driving these ion exchange reactions. The findings have important implications for understanding the bioavailability and stability of these mineral supplements and fortified food products.

Received 7th July 2025
Accepted 13th October 2025

DOI: 10.1039/d5ra04858c

rsc.li/rsc-advances

1. Introduction

Calcium and iron are essential metals for human health, but their dietary intake and absorption are often insufficient, leading to disorders such as osteoporosis, hypertension, cardiovascular disease, and anemia.[1] Food fortification with calcium and iron hydroxycarboxylates, such as lactate and gluconate, is a widely accepted strategy to enhance their bioavailability.[2,3] However, the bioavailability of these minerals depends on their solubility and speciation in aqueous solutions, which can be influenced by various factors such as pH, temperature, and the presence of other ions or molecules.[4,5] Moreover, the interactions between calcium and iron in food matrices and in the human body are complex and not fully understood.[6] For example, iron can affect the solubility and precipitation of calcium salts, such as carbonate,[7,8] phosphate,[9] and hydroxyapatite,[10] which are important for bone mineralization. Iron can also form binuclear complexes with calcium and gluconate, which may alter the redox potential of iron and reduce its oxidative damage.[11] As iron supplementation becomes increasingly common, understanding its impact on calcium homeostasis is of importance.[12] This necessitates a comprehensive investigation into the thermodynamics and kinetics of dissolution and complexation reactions involving calcium and iron(II) hydroxycarboxylates in aqueous solutions.

Accordingly, the present study aims to elucidate the effects of iron on calcium solubility, speciation, complexation, and mineralization. We focused on calcium and iron(II) hydroxycarboxylates, examining their individual and combined behaviors in aqueous solutions. Using a multifaceted approach, we employed electrochemical methods and density functional theory calculations to investigate the aqueous dissolution of these compounds at various temperatures. Furthermore, we characterized the influence of iron on calcium solubility, calcium ion activity, binding constants, competitive interactions, and complex formation across different calcium and iron(II) hydroxycarboxylates combinations. For the mixed systems, we investigated further, examining supersaturation phenomena, precipitation kinetics, and the interplay of thermodynamic and kinetic driving forces.

The findings provide valuable insights for the design and optimization of mineral supplements and fortificants, addressing a critical need in nutritional science and pharmaceutical development. Moreover, our results contribute to the broader understanding of mineral metabolism and homeostasis in biological systems. By unraveling the complex interactions between calcium and iron(II) hydroxycarboxylates, this

[a]*College of Food Science and Nutritional Engineering, China Agricultural University, Beijing 100083, China. E-mail: ningtang@cau.edu.cn; Tel: +86-010-62737401*
[b]*Beijing Key Laboratory of Functional Food from Plant Resources, Beijing 100083, China*

study paves the way for more effective strategies in managing calcium balance, particularly in the context of iron supplementation, ultimately supporting better bone health and overall well-being.

2. Materials and methods

2.1 Chemicals

Calcium L-lactate pentahydrate, calcium D-gluconate monohydrate (purity ≥ 98%), iron(II) lactate hydrate (purity ≥ 98%), iron(II) D-gluconate dehydrate (purity ≥ 98%), calcium chloride dihydrate (purity ≥ 99%), iron(II) chloride tetrahydrate (purity ≥ 98%), and murexide were all purchased from Sigma-Aldrich (Shanghai, China). Ethylenediaminetetraacetic acid disodium salt dihydrate (EDTA) (purity ≥ 99%) and sodium hydroxide were from Solarbio (Beijing, China). All the other chemicals were of analytical grade and used without further purification.

2.2 Methods

This study employed a comprehensive set of analytical and computational techniques to investigate the properties and interactions of calcium and iron hydroxycarboxylates. The primary methods included solubility determination, electric conductivity measurements, and density functional theory (DFT) calculations. Structural and spectroscopic analyses were performed using X-ray diffraction (XRD) and Fourier transform infrared (FTIR) spectroscopy. Thermodynamic properties were assessed through isothermal titration calorimetry (ITC). A series of mixed solutions were prepared and analyzed to explore the interactions between various combinations of calcium and iron(II) compounds. These included mixed solutions of calcium hydroxycarboxylates with iron(II) chloride, calcium L-lactate with iron(II) lactate, calcium D-gluconate with iron(II) D-gluconate, calcium L-lactate with iron(II) D-gluconate, and calcium D-gluconate with iron(II) lactate. The total calcium concentrations were determined using EDTA titration, while iron(II) concentrations were measured *via* $KMnO_4$ titration. Detailed procedures for each experimental method, including solution preparation, instrumental parameters, and analytical protocols, are provided in the SI.[13–20]

3. Results and discussion

3.1 Solubility and speciation of calcium and iron(II) hydroxycarboxylates

The aqueous solubility of calcium and iron(II) hydroxycarboxylates was investigated at temperatures of 25 °C, 37 °C, and 49 °C in relation to their potential bioavailability. Experimental results, as presented in Table 1, demonstrated that the solubility of both calcium and iron(II) hydroxycarboxylates increased with rising temperature, confirming previous reports on calcium salt solubility.[21,22] Accordingly, the overall dissolution process for each calcium and iron(II) hydroxycarboxylate was determined to be endothermic $\Delta H > 0$, consistent with the behavior of most food-related calcium and iron(II) salts in aqueous solutions. For calcium salts, calcium lactate exhibited higher solubility (6.49 ± 0.08 g/100 mL at 25 °C) compared to calcium gluconate (3.64 ± 0.03 g/100 mL at 25 °C) ($p < 0.05$). Both calcium salts demonstrated similar temperature sensitivity, with a solubility ratio of 2.2. The solubility ratio, calculated by dividing the highest solubility by the lowest solubility, quantifies the degree of variation in hydroxycarboxylate solubility with temperature.

Interestingly, the solubility trend for iron(II) hydroxycarboxylates differed from that of calcium salts. Iron(II) lactate (1.77 ± 0.02 g/100 mL at 25 °C) showed lower solubility than iron(II) gluconate (9.81 ± 0.02 g/100 mL at 25 °C) ($p < 0.05$). This contrasting behavior can be attributed to several factors. Calcium, being a larger ion with a lower charge density compared to iron(II), generally forms weaker complexes with ligands.[23] This tendency often results in higher solubility for calcium salts. Iron(II), with its smaller ionic radius and higher charge density, forms stronger complexes with both lactate and gluconate compared to calcium. The stronger metal–ligand interactions in iron(II) complexes generally lead to lower solubility. However, the significant size difference between lactate and gluconate introduces an additional factor. The much larger gluconate ion, when complexed with iron(II), creates a more disordered structure that is harder to pack efficiently in a crystal lattice. This disorder increases the solubility of iron(II) gluconate substantially. In terms of temperature sensitivity, iron(II) lactate, being less soluble, exhibited the lowest temperature sensitivity with a solubility ratio of 1.5. In contrast, iron(II) gluconate demonstrated a higher temperature sensitivity, with a solubility ratio of 2.5. This indicated that iron(II) gluconate might become available more quickly as they enter the warmer environment of the body, potentially affecting absorption kinetics.

As temperature increased, the solubility of these compounds significantly rose, as previously discussed.[24,25] However, a contrasting trend emerged for ion activity in saturated solutions: it decreased with increasing temperature, despite the higher solubility (Table 1). This result was consistent with previous studies on calcium hydroxycarboxylates, which also observed increased solubility but decreased calcium ion activity with increasing temperature ($p < 0.05$).[17] This seemingly paradoxical behavior suggested a complex dissolution process involving stepwise dissociation and complex formation:

$$ML_2 \rightleftharpoons ML^+ + L^- \quad (1)$$

$$ML^+ \rightleftharpoons M^{2+} + L^- \quad (2)$$

where M represents the metal ion (Ca^{2+} or Fe^{2+}) and L represents the hydroxycarboxylate ligand (lactate or gluconate). Notably, the determined ion activity was calculated based on the measured electronic conductivity.[14] As reactions (1) and (2) were observed to result in complete dissociation into M^{2+}, the dissociation degree (α_{dis}) could be first calculated using the electrical conductivity according to the following equation to quantify this behavior:

$$\alpha_{dis} = \frac{\Lambda}{c_{M^{2+}} \Lambda_\infty} \quad (3)$$

Table 1 The pH, solubility, total calcium/iron(II) concentration ($c_{Ca^{2+}}/c_{Fe^{2+}}$), calculated calcium/iron(II) ion activity ($\alpha_{Ca^{2+}}/\alpha_{Fe^{2+}}$), ionic strength ($I$), calcium/iron(II) ion activity coefficient ($\gamma_{Ca^{2+}}/\gamma_{Fe^{2+}}$), calculated free calcium/iron(II) concentration ($[Ca^{2+}]/[Fe^{2+}]$), calculated metal–ligand complex concentration ($[CaL^{+}]/[FeL^{+}]$), calculated free hydroxycarboxylate ion concentration($[L^{-}]$), solubility products based on the concentration ($K_{sp,c}$) and activity ($K_{sp,\alpha}$), and association constants based on the conductivity (K_c) and activity (K_a) of saturated calcium L-lactate, calcium D-gluconate, iron(II) lactate, and iron(II) D-gluconate in aqueous solutions at 25, 37, and 49 °C. Data are expressed as mean ± SD from three independent experiments and three replicates

Sample	T (°C)	Solubility (g/100 mL)	$c_{Ca^{2+}}/c_{Fe^{2+}}$ (mol L^{-1})	$\alpha_{Ca^{2+}}/\alpha_{Fe^{2+}}$	I	$\gamma_{Ca^{2+}}/\gamma_{Fe^{2+}}$	$[Ca^{2+}]/[Fe^{2+}]$ (mol L^{-1})	$[CaL^{+}]/[FeL^{+}]$ (mol L^{-1})	$[L^{-}]$ (mol L^{-1})	$K_{sp,c}$	$K_{sp,\alpha}$	K_c	K_a
Calcium L-lactate	25 °C	6.49 ± 0.08	0.297 ± 0.003	(8.7 ± 0.1) × 10^{-4}	0.3060 ± 0.0001	0.28887 ± 0.00001	(3.00 ± 0.05) × 10^{-3}	0.2970 ± 0.0001	0.3030 ± 0.0001	(2.75 ± 0.05) × 10^{-4}	(4.27 ± 0.05) × 10^{-5}	327 ± 5	1131 ± 20
	37 °C	9.43 ± 0.4	0.43 ± 0.02	(7.98 ± 0.07) × 10^{-4}	0.43 ± 0.02	0.2791 ± 0.0006	(2.86 ± 0.03) × 10^{-3}	0.43 ± 0.02	0.43 ± 0.02	(5.2 ± 0.5) × 10^{-4}	(7.7 ± 0.6) × 10^{-5}	345 ± 4	1236 ± 12
	49 °C	14.1 ± 0.2	0.645 ± 0.007	(7.1 ± 0.2) × 10^{-4}	0.650 ± 0.007	0.289 ± 0.001	(2.45 ± 0.06) × 10^{-3}	0.643 ± 0.007	0.647 ± 0.007	(1.029 ± 0.004) × 10^{-3}	(1.6046 ± 0.0008) × 10^{-4}	404 ± 11	1396 ± 31
Calcium D-gluconate	25 °C	3.64 ± 0.03	0.0845 ± 0.0007	(8.01 ± 0.01) × 10^{-4}	0.0887 ± 0.0006	0.3856 ± 0.0008	(2.10 ± 0.02) × 10^{-3}	0.0824 ± 0.0007	0.0866 ± 0.0006	(1.575 ± 0.007) × 10^{-5}	(3.77 ± 0.01) × 10^{-6}	453 ± 4	1175 ± 17
	37 °C	5.1 ± 0.2	0.118 ± 0.003	(7.13 ± 0.06) × 10^{-4}	0.12415 ± 0.00004	0.34319 ± 0.00003	(2.07 ± 0.02) × 10^{-3}	0.11793 ± 0.00002	0.12207 ± 0.00002	(3.089 ± 0.003) × 10^{-5}	(6.26 ± 0.06) × 10^{-6}	466 ± 5	1355 ± 13
	49 °C	8.0 ± 0.3	0.185 ± 0.007	(5.9 ± 0.2) × 10^{-4}	0.1940 ± 0.0001	0.29525 ± 0.00005	(2.00 ± 0.07) × 10^{-3}	0.1880 ± 0.0001	0.1920 ± 0.0001	(7.4 ± 0.3) × 10^{-5}	(1.18 ± 0.04) × 10^{-5}	490 ± 17	1661 ± 58
Iron(II) lactate	25 °C	1.77 ± 0.02	0.0755 ± 0.0007	(7.9 ± 0.2) × 10^{-4}	0.0795 ± 0.0001	0.3981 ± 0.0001	(1.99 ± 0.05) × 10^{-3}	0.07351 ± 0.00005	0.07749 ± 0.00005	(1.50 ± 0.09) × 10^{-6}	(3.00 ± 0.07) × 10^{-6}	475 ± 13	1196 ± 32
	37 °C	2.25 ± 0.09	0.096 ± 0.007	(7.3 ± 0.3) × 10^{-4}	0.10 ± 0.0002	0.3662 ± 0.0002	(1.94 ± 0.07) × 10^{-3}	0.09406 ± 0.00007	0.09794 ± 0.00008	(1.86 ± 0.08) × 10^{-6}	(4.1 ± 0.1) × 10^{-6}	496 ± 20	1354 ± 55
	49 °C	2.67 ± 0.003	0.114 ± 0.0002	(5.8 ± 0.1) × 10^{-4}	0.11742 ± 0.00008	0.33824 ± 0.00007	(1.71 ± 0.04) × 10^{-3}	0.11229 ± 0.00004	0.11571 ± 0.00004	(2.29 ± 0.06) × 10^{-6}	(4.5 ± 0.1) × 10^{-6}	568 ± 15	1679 ± 43
Iron(II) D-gluconate	25 °C	9.81 ± 0.02	0.22 ± 0.0004	(6.0 ± 0.2) × 10^{-4}	0.2240 ± 0.0002	0.30322 ± 0.00004	(1.98 ± 0.09) × 10^{-3}	0.2180 ± 0.0001	0.2220 ± 0.0001	(9.8 ± 0.5) × 10^{-5}	(1.63 ± 0.08) × 10^{-5}	497 ± 23	1638 ± 75
	37 °C	15.5 ± 0.6	0.35 ± 0.01	(5.0 ± 0.3) × 10^{-4}	0.35 ± 0.01	0.2794 ± 0.0006	(1.8 ± 0.1) × 10^{-3}	0.35 ± 0.01	0.35 ± 0.01	(2.21 ± 0.02) × 10^{-4}	(3.26 ± 0.02) × 10^{-5}	555 ± 41	1988 ± 151
	49 °C	23.4 ± 0.5	0.52 ± 0.01	(4.1 ± 0.01) × 10^{-4}	0.52299 ± 0.00002	0.27394 ± 0.00001	(1.50 ± 0.01) × 10^{-3}	0.51850 ± 0.00001	0.52149 ± 0.00001	(4.07 ± 0.02) × 10^{-4}	(5.83 ± 0.04) × 10^{-5}	665 ± 5	2426 ± 18

where Λ is the electrical conductivity and $c_{M^{2+}}$ is the concentration of total calcium or iron(II). From this, the concentration-based dissociation constant K'_{ads} and association constant K_c can be obtained using the following equations:

$$K'_{dis} = \frac{{\alpha_{dis}}^2}{(1-\alpha_{dis})} \times c_{M^{2+}} \quad (4)$$

$$K_c = \frac{1}{K'_{dis}} = \frac{[ML^+]}{[M^{2+}][L^-]} \quad (5)$$

where $[ML^+]$ represents the concentration of the 1 : 1 complex, $[L^-]$ is the free concentration of lactate or gluconate, and $[M^{2+}]$ is the free concentration of calcium or iron(II) ions, calculated using ion activity:

$$[M^{2+}] = \frac{\alpha_{M^{2+}}}{\gamma^{2+}} \quad (6)$$

where γ^{2+} is the activity coefficient calculated using the Davies equation:

$$\log \gamma^{2+} = -A_{DH} z^2 \left(\frac{\sqrt{I}}{1+\sqrt{I}} - 0.3I \right) \quad (7)$$

where A_{DH} is the Debye–Hückel constant (0.51, 0.519, or 0.535 at 25, 37, or 49 °C, respectively), z is the ion charge, and I is the ionic strength. Ionic strength was calculated considering all ions present, including the formed complexes:

$$I = \tfrac{1}{2}\sum cz^2 = \tfrac{1}{2}(4[M^{2+}] + [L^-] + [ML^+]) \quad (8)$$

$$[L^-] = c_{M^{2+}} + [M^{2+}] = c_{M^{2+}} + \frac{\alpha_{M^{2+}}}{\gamma^{2+}} \quad (9)$$

$$[ML^+] = c_{M^{2+}} - [M^{2+}] = c_{M^{2+}} - \frac{\alpha_{M^{2+}}}{\gamma^{2+}} \quad (10)$$

Based on the eqn (6)–(10), the K_c can be reorganized into a quadratic equation of $\alpha_{M^{2+}}$.

$$K_c = \frac{[ML^+]}{[M^{2+}][L^-]} = \frac{c_{M^{2+}} - \frac{\alpha_{M^{2+}}}{\gamma^{2+}}}{\frac{\alpha_{M^{2+}}}{\gamma^{2+}} \times \left(c_{M^{2+}} + \frac{\alpha_{M^{2+}}}{\gamma^{2+}} \right)} \quad (11)$$

An iterative calculation was then performed, starting with an assumed ionic strength of $3c_{M^{2+}}$. This process continued until the ionic strength derived from eqn (8) reached a stable value. Then the concentration-based association constant can be further corrected to thermodynamic association constant (K_a):

$$K_a = \frac{K_c}{\gamma^{2+}} \quad (12)$$

The speciation of the investigated hydroxycarboxylates, as determined by the iterative calculation procedure described above, is presented in Table 1. Our analysis revealed that gluconate formed stronger complexes than lactate with both calcium and iron(II). At 25 °C, the K_a values for calcium and iron(II) gluconate complexes were 1175 ± 17 and 1638 ± 75, respectively, compared to 1131 ± 20 and 1196 ± 32 for the corresponding lactate complexes. The order of complex strength for calcium binding aligned with the existing studies.[17] Notably, iron(II) exhibited stronger binding to both hydroxycarboxylates compared to calcium ($p < 0.05$), as evidenced by the higher association constants. These findings highlighted the complex interplay between temperature, solubility, and speciation, which is crucial for understanding these compounds' behavior under various physiological conditions.

3.2 Thermodynamic analysis of calcium and iron(II) hydroxycarboxylates

The temperature dependence of thermodynamic association constants was further analyzed using the van't Hoff equation to determine the standard enthalpy (ΔH_a°) and entropy (ΔS_a°) of complex formation:[26]

$$\ln K_a = -\frac{\Delta H_a^\circ}{RT} + \frac{\Delta S_a^\circ}{R} \quad (13)$$

The linear fit of the van't Hoff plot (Fig. 1) confirmed the validity of the iterative calculation procedure. The thermodynamic parameters (Table 2), calculated from eqn (13), yielded $\Delta H_a^\circ > 0$ and $\Delta S_a^\circ > 0$, indicating an endothermic and entropy-driven complex formation process. Since the complex formation is endothermic corresponding to $\Delta H_a^\circ > 0$, a process of energy consumption, the complex formation must be entropy driven with $\Delta S_a^\circ > 0$. The positive entropy change may be attributed to the release of water molecules bound to the cation and carboxyl groups during complex formation.[27] The thermodynamic analysis of hydroxycarboxylate complexes with calcium and iron(II), conducted in saturated aqueous solutions, yielded association constants and derived parameters with broad applicability due to their basis in ion activity rather than concentration. This approach enhanced the universal relevance of the findings for various aqueous environments. To elucidate the structural effects on calcium and iron(II) binding across the hydroxycarboxylates, quantum mechanical calculations were performed using density functional theory (DFT).[28] This computational approach optimized the structures of calcium and iron(II) complexes in aqueous solution and calculated the binding enthalpy ($\Delta H_{binding}$) for the complexation reactions, accounting for solvent interactions. The obtained $\Delta H_{binding}$ values are included in Table 2. The ordering of affinity of calcium and iron(II) ion to hydroxycarboxylates was in agreement with the experimentally determined values for K_a. Furthermore, the relative strength of binding of calcium to D-gluconate and L-lactate was 1.2, and iron(II) to D-gluconate and lactate was 1.4, which were close to the ratio indicated by the experimentally determined values for K_a. The optimized structures of the complexes are presented in Fig. 2. In L-lactate complexes, both calcium and iron(II) ions exhibited bidentate binding, interacting exclusively with the oxygen atoms of the carboxylate group.[29] The bond lengths for these interactions were approximately 2.4 Å for calcium–oxygen and 1.95 Å for iron(II)–oxygen. In contrast, D-gluconate complexes

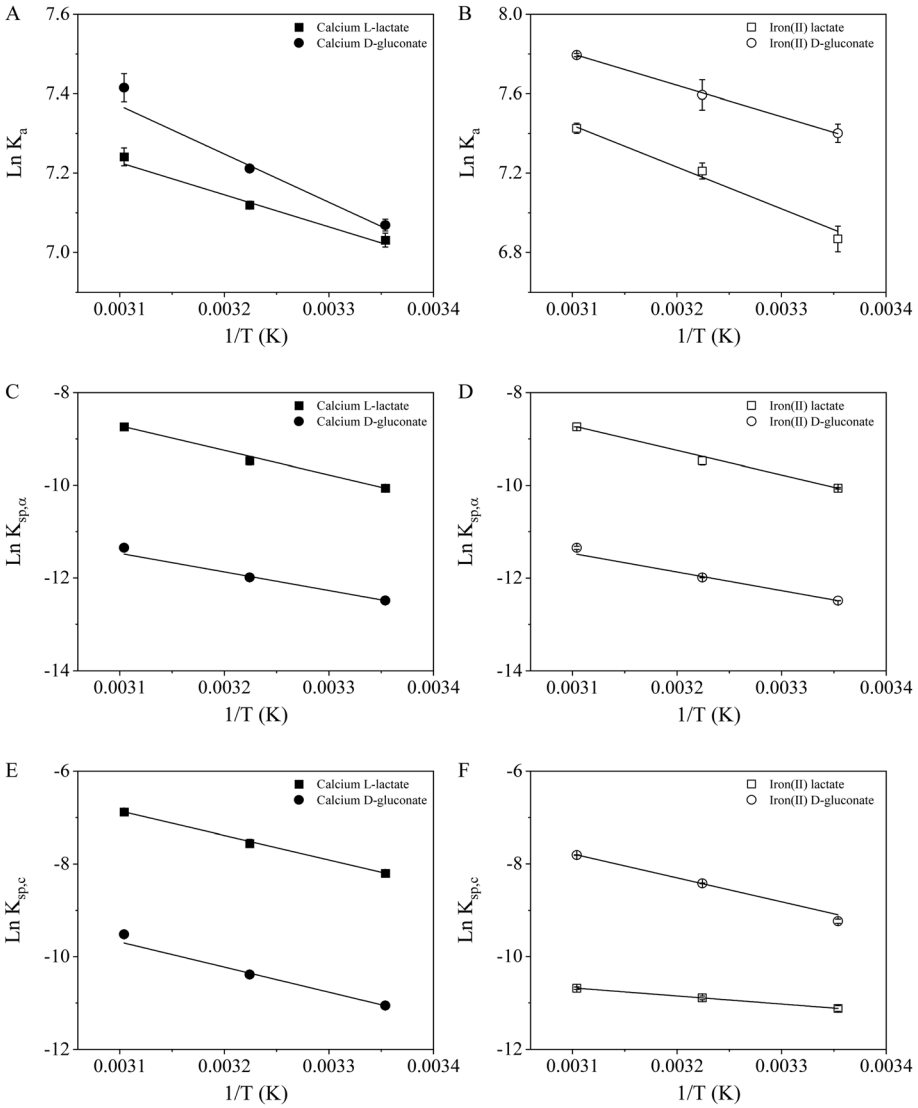

Fig. 1 Temperature dependence of various thermodynamic parameters for calcium and iron(II) hydroxycarboxylates in aqueous solutions. Effect of temperature on the thermodynamic association constant (K_a) for calcium (A) and iron(II) hydroxycarboxylates (B), respectively. The influence of temperature on solubility products is presented in two ways, $K_{sp,\alpha}$, calculated based on the activity of calcium (C) and iron(II) hydroxycarboxylates (D), $K_{sp,c}$, calculated based on the concentration of calcium (E) and iron(II) hydroxycarboxylates (F).

demonstrated a more complex tridentate binding mode for both metal ions. Here, the binding involved one carboxylate oxygen and the hydroxyl groups at C-2 and C-4 positions. Interestingly, the bond lengths in D-gluconate complexes remained consistent with those observed in L-lactate: about 2.4 Å for calcium–oxygen and 1.95 Å for iron-oxygen. The difference in binding modes between L-lactate and D-gluconate complexes appeared to have significant implications for binding strength. The tridentate binding observed in calcium D-gluconate and iron(II) D-gluconate complexes seemed to result in stronger binding compared to the bidentate mode seen in lactate complexes. In addition, the stronger iron binding to lactate and gluconate correlated with shorter bond lengths, consistent with previous studies on metal–ligand interactions.[30]

The solubility product constants of calcium and iron(II) hydroxycarboxylates were calculated using the information provided in Table 1, which detailed their forms in saturated solutions. Both the thermodynamic solubility product ($K_{sp,\alpha}$), based on activity, and the concentration-based solubility product ($K_{sp,c}$) were determined using eqn (14) and (15), respectively. These calculations were performed for calcium lactate, calcium gluconate, iron(II) lactate, and iron(II) gluconate at three different temperatures.

$$K_{sp,\alpha} = \alpha_{M^{2+}}\alpha_{L^-}{}^2 = \gamma_{M^{2+}}\gamma_{L^-}{}^2[M^{2+}][L^-]^2 \quad (14)$$

$$K_{sp,c} = [M^{2+}][L^-]^2 \quad (15)$$

Subsequent analysis of the thermodynamic properties (Table 2), derived from the van't Hoff equation (Fig. 1), revealed intriguing differences in the dissolution processes of these compounds. For calcium compounds, calcium L-lactate

Table 2 Thermodynamic parameters for calcium/iron(II) hydroxycarboxylate complexes and their dissolution. The ΔH_a, ΔS_a, and ΔG_a for 1 : 1 calcium/iron(II) hydroxycarboxylates complexes, calculated using the van't Hoff equation with activity-based association constants (K_a), and binding enthalpy ($\Delta H_{binding}$) from DFT calculations. The ΔH_{dis}, ΔS_{dis}, and ΔG_{dis} for the dissolution of calcium and iron(II) hydroxycarboxylates calculated using the van't Hoff equation with activity-based solubility product ($K_{sp,\alpha}$) and concentration-based solubility product ($K_{sp,c}$) (refer to Table 1). The $\Delta H_{dis}(Q)$, $\Delta S_{dis}(Q)$, and $\Delta G_{dis}(Q)$ for the dissolution of homologous (same anions) calcium and iron(II) hydroxycarboxylates mixtures calculated using with activity-based ionic product ($Q_{sp,\alpha}$) (refer to Table 3) and concentration-based ionic product ($Q_{sp,c}$) (refer to Table 3)

Salts	ΔH_a° (kJ mol^{-1})	ΔS_a° (J mol^{-1} K^{-1})	ΔG_a° (kJ mol^{-1})	$\Delta H_{binding}$ (kJ mol^{-1})	$\Delta H_{dis,\alpha}$ (kJ mol^{-1})	$\Delta S_{dis,\alpha}$ (J mol^{-1} K^{-1})	$\Delta G_{dis,\alpha}$ (kJ mol^{-1})	$\Delta H_{dis,c}$ (kJ mol^{-1})	$\Delta S_{dis,c}$ (J mol^{-1} K^{-1})	$\Delta G_{dis,c}$ (kJ mol^{-1})	$\Delta H_{dis,\alpha}(Q)$ (kJ mol^{-1})	$\Delta S_{dis,\alpha}(Q)$ (J mol^{-1} K^{-1})	$\Delta G_{dis,\alpha}(Q)$ (kJ mol^{-1})	$\Delta H_{dis,c}(Q)$ (kJ mol^{-1})	$\Delta S_{dis,c}(Q)$ (J mol^{-1} K^{-1})	$\Delta G_{dis,c}(Q)$ (kJ mol^{-1})
Calcium L-lactate	6.0 ± 0.6	79 ± 2	−17.41 ± 0.05	−126.13	43.9 ± 0.6	63 ± 2	25.01 ± 0.03	43.8 ± 0.8	79 ± 3	20.35 ± 0.03	43 ± 2	62 ± 5	24.78 ± 0.04	41 ± 1	71 ± 5	20.08 ± 0.04
Calcium D-gluconate	12 ± 3	98 ± 11	−17.49 ± 0.01	−150.22	38 ± 1	23 ± 4	31.03 ± 0.02	51 ± 1	79 ± 4	27.5 ± 0.03	51 ± 3	69 ± 10	30.6 ± 0.1	53 ± 3	92 ± 10	26.0 ± 0.2
Iron(II) lactate	11.24 ± 0.02	96.5 ± 0.2	−17.52 ± 0.08	−278.18	13.51 ± 0.01	−60.0 ± 0.1	31.40 ± 0.03	15 ± 1	−44 ± 4	27.6 ± 0.2	36 ± 2	18 ± 5	30.72 ± 0.06	34 ± 2	27 ± 6	26.03 ± 0.07
Iron(II) D-gluconate	13 ± 2	105 ± 5	−18.35 ± 0.16	−393.49	43 ± 2	51 ± 6	27.3 ± 0.1	48 ± 2	83 ± 6	22.8 ± 0.1	47 ± 2	66 ± 8	27.5 ± 0.1	49 ± 2	89 ± 7	22.9 ± 0.1

demonstrated higher enthalpy and entropy of dissolution based on $K_{sp,\alpha}$ compared to calcium D-gluconate (Table 2). This observation suggested that the dissolution process of calcium L-lactate was more endothermic and led to a greater increase in system disorder. Interestingly, calcium L-lactate also exhibited a lower Gibbs free energy of dissolution, indicating that its dissolution was more thermodynamically favorable. These findings implied that despite the higher energy requirement for dissolution, the process was driven by the significant increase in entropy, ultimately resulting in a more spontaneous reaction. In contrast to the calcium compounds, iron(II) lactate displayed lower enthalpy and entropy of dissolution compared to iron(II) D-gluconate (Table 2). This indicated that the dissolution of iron(II) lactate was less endothermic and resulted in a more ordered system. However, the higher Gibbs free energy of dissolution for iron(II) lactate suggested that its dissolution process was less thermodynamically favorable. The contrasting behavior of lactate and gluconate ligands when complexed with calcium *versus* iron(II) underscored the importance of considering metal–ligand interactions in predicting and understanding solubility trends. The more favorable dissolution of calcium L-lactate compared to calcium D-gluconate may be attributed to differences in their crystal structures or hydration patterns.[31] The higher entropy gain during calcium L-lactate dissolution suggested a greater disruption of the solid-state structure or a more extensive hydration of the dissolved species. For the iron compounds, the less favorable dissolution of iron(II) lactate despite its lower enthalpy of dissolution was particularly intriguing. This could potentially be explained by stronger ion-pairing in solution or a more stable crystal lattice that resisted dissolution. The lower entropy change for iron(II) lactate dissolution might indicate a more structured solvation shell around the dissolved species, which could contribute to the less favorable overall process. Understanding the thermodynamic factors governing the dissolution of these compounds could aid in predicting their behavior in different physiological

Fig. 2 Optimized structures of 1 : 1 calcium L-lactate, calcium D-gluconate, iron(II) lactate, and iron(II) D-gluconate complexes, calculated using density functional theory (B3LYP/6-311G(d,p)) combined with the polarizable continuum model using the integral equation formalism variant (IEFPCM).

environments and guide the selection of appropriate forms for specific applications.

3.3 Effect of $FeCl_2$ on calcium ion activity and solubility of calcium hydroxycarboxylates

The influence of iron(II) chloride on the calcium ion activity and solubility of calcium lactate and calcium gluconate was investigated in relation to the complex interplay between different ionic species in aqueous solutions. The results were illustrated in Fig. 3A and B. At low concentrations, iron(II) chloride had no significant impact on the solubility of both calcium salts, suggesting a threshold effect. However, as the concentration of iron(II) chloride increased, a marked enhancement in the solubility of calcium hydroxycarboxylates was observed ($p < 0.05$), indicating a significant alteration in the solution's thermodynamic landscape.

This phenomenon could be explained through several potential mechanisms. The addition of iron(II) chloride increases the total ionic concentration in the solution, enhancing inter-ionic interactions. This elevation in ionic strength may reduce the propensity for anions to combine with calcium ions and form molecules, leading to increased solute dissolution.[8] Additionally, iron(II) chloride may compete with calcium ions for complexation with lactate or gluconate ligands. Given that iron(II) ions typically form stronger complexes than calcium ions with these ligands, this competition could result in the displacement of calcium from its complexes, thereby increasing the free calcium ion concentration.[32] The observed increase in calcium hydroxycarboxylate solubility aligned with previous studies demonstrating that iron(II) ions inhibited calcium carbonate crystallization and enhanced hydroxyapatite dissolution.[7,33] This suggested a broader role for iron(II) ions in interfering with calcium salt precipitation and promoting dissolution. Fig. 3C and D further supported these findings, showing a slight increase in calcium ion activity with the addition of iron(II) ions, as determined by calcium ion-selective electrode measurements.

3.4 Ionic interactions in mixed calcium and iron(II) hydroxycarboxylates solutions

The bioavailability of these minerals can be significantly influenced by their chemical environment and interactions with other nutrients.[34,35] Of particular interest is the potential impact of iron on calcium absorption and utilization in the body. Understanding the thermodynamic behavior of these mineral complexes can help in developing more bioavailable forms of calcium and iron supplements, potentially improving their efficacy. Furthermore, the gastrointestinal environment often contains a mix of different mineral salts, making the study of mixed calcium and iron(II) salt solutions important for understanding nutrient absorption *in vivo*.[36,37] To investigate these complex interactions, we examined the thermodynamic properties of calcium L-lactate, calcium D-gluconate, iron(II) lactate, and iron(II) D-gluconate. These compounds serve as

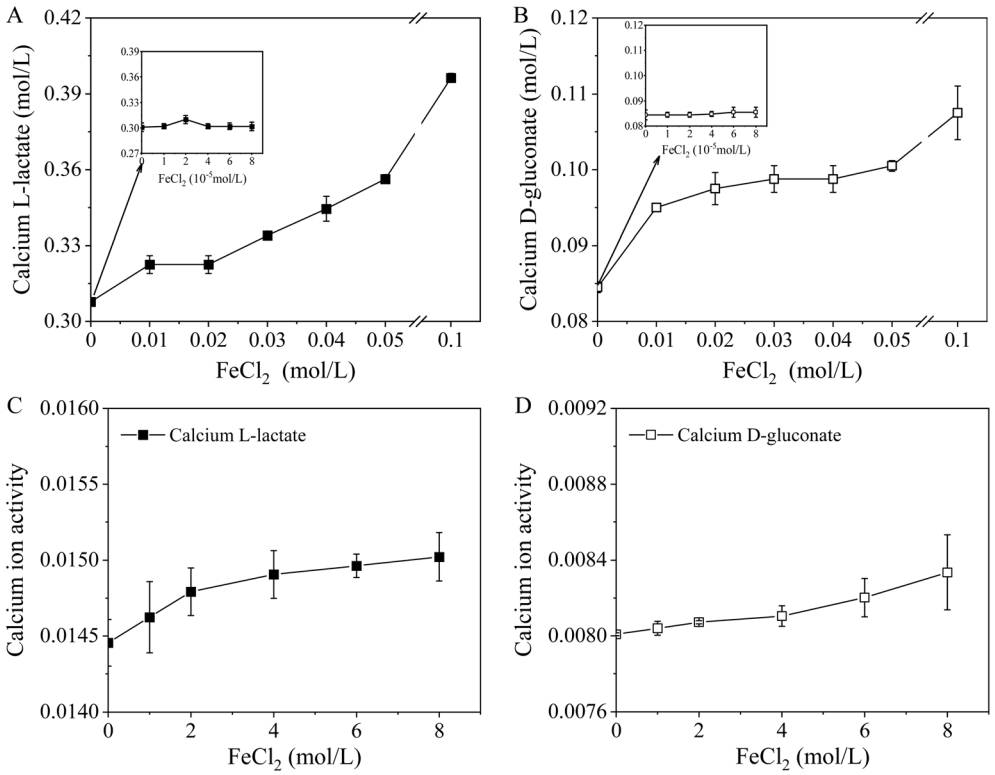

Fig. 3 Effect of ferrous chloride addition on the total calcium concentration and calcium ion activity in solutions containing calcium L-lactate (A and C) and calcium D-gluconate (B and D), respectively.

models for understanding how iron(II) hydroxycarboxylates affect the thermodynamic equilibrium state of calcium salts, which in turn can influence their bioavailability. Four mixed systems were studied: $CaLac_2$ + $FeLac_2$, $CaGlu_2$ + $FeGlu_2$, $CaGlu_2$ + $FeLac_2$, and $CaLac_2$ + $FeGlu_2$. These systems can be categorized into two groups based on the nature of their ionic interactions:

(1) Homologous systems ($CaLac_2$ + $FeLac_2$ and $CaGlu_2$ + $FeGlu_2$): These combinations involve the same anion and do not exhibit competitive binding between ions.

(2) Cross-ligand systems ($CaGlu_2$ + $FeLac_2$ and $CaLac_2$ + $FeGlu_2$): These combinations involve different anions, leading to competitive binding of ions during the dissolution process.

By studying these systems, we aim to elucidate how different ligands and ionic interactions might affect the solubility, stability, and potential bioavailability of calcium and iron in mixed solutions.

3.4.1 Thermodynamic behavior of homologous mixed systems: $CaLac_2$ + $FeLac_2$ and $CaGlu_2$ + $FeGlu_2$. The ionic partitioning in homologous mixed systems was investigated through an iterative calculation process based on the equilibrium constants (K_c) presented in Table 1 and the measured total calcium and iron concentrations in the equilibrium solutions. The calculations were performed using eqn (16)–(21),

$$T_{L^-} = [FeL^+] + [CaL^+] + [L^-] = 2(c_{Ca^{2+}} + c_{Fe^{2+}}) \quad (16)$$

$$[Ca^{2+}] = \frac{[CaL^+]}{K_{CaL_2,c}[L^-]} \quad (17)$$

$$[CaL^+] = c_{Ca^{2+}} - [Ca^{2+}] \quad (18)$$

$$[Fe^{2+}] = \frac{[FeL^+]}{K_{FeL_2,c}[L^-]} \quad (19)$$

$$[FeL^+] = c_{Fe^{2+}} - [Fe^{2+}] \quad (20)$$

$$[L^-] = c_{Ca^{2+}} + c_{Fe^{2+}} + [Ca^{2+}] + [Fe^{2+}] \quad (21)$$

where T_{L^-} represents the total lactate or gluconate concentration. Table 3 illustrates the ion speciation in the clarified $CaLac_2$ + $FeLac_2$ and $CaGlu_2$ + $FeGlu_2$ mixed solutions. Upon mixing and dissolution of these salts, a notable decrease in the solubilities of both calcium and iron(II) hydroxycarboxylates was observed. This phenomenon could be attributed to the increased concentration of Lac^- or Glu^- in the system, which suppressed the ionization of the electrolytes. Consequently, the dissociation processes described by eqn (1) and (2) were inhibited. The linear relationship observed in the van't Hoff plots (Fig. 4) not only provided thermodynamic parameters (Table 2) but also validated the ion speciation calculations (Table 3).

In the $CaLac_2$ + $FeLac_2$ system, iron(II) ions form stronger complexes with lactate compared to calcium ions. Additionally, iron(II) lactate exhibited the lowest solubility among the salts studied. These factors contribute to a higher propensity for $FeLac_2$ precipitation as $[Lac^-]$ increased:

Table 3 Total calcium/iron(II) concentration ($c_{Ca^{2+}}/c_{Fe^{2+}}$), speciation (calculated free calcium/iron(II) concentration ($[Ca^{2+}]/[Fe^{2+}]$), calculated calcium/iron(II) hydroxycarboxylates complex concentration ($[CaL^+]/[FeL^+]$)), total hydroxycarboxylates concentration (T_{L^-}), ionic strengths (I), ion activities ($\alpha_{Ca^{2+}}$, $\alpha_{Fe^{2+}}$, and α_{L^-}), and ionic products based on concentration (Q_c) or activity (Q_α) for the dissolution of calcium lactate and iron(II) lactate mixtures and calcium gluconate and iron(II) gluconate mixtures at 25, 37, and 49 °C. Data are expressed as mean ± SD from three independent experiments and three replicates

Ligand	T (°C)	$c_{Ca^{2+}}$	$c_{Fe^{2+}}$	$[Ca^{2+}]$	$[Fe^{2+}]$	$[CaL^+]$	$[FeL^+]$	T_{L^-}	I	$\alpha_{Ca^{2+}}$	$\alpha_{Fe^{2+}}$	α_{L^-}	$Q_{Ca,c}$	$Q_{Fe,c}$	$Q_{Ca,\alpha}$	$Q_{Fe,\alpha}$
Lactate	25	0.298 ± 0.040		(2.65 ± 0.01) × 10^{-3}	(2.43 ± 0.09) × 10^{-4}	0.295 ± 0.039		0.67 ± 0.343		(7.59 ± 0.04) × 10^{-4}	(7.0 ± 0.2) × 10^{-5}	0.249 ± 0.004	(3.07 ± 0.09) × 10^{-4}	(2.8 ± 0.2) × 10^{-5}	(4.7 ± 0.1) × 10^{-5}	(4.3 ± 0.3) × 10^{-6}
		0.004	0.002			0.004	0.002	0.01	0.006							
	37	0.418 ± 0.048		(2.57 ± 0.1) × 10^{-3}	(2.1 ± 0.1) × 10^{-4}	0.415 ± 0.048		0.93 ± 0.471		(7.21 ± 0.04) × 10^{-4}	(5.8 ± 0.4) × 10^{-5}	0.341 ± 0.005	(5.6 ± 0.1) × 10^{-4}	(4.5 ± 0.4) × 10^{-5}	(8.4 ± 0.2) × 10^{-5}	(6.7 ± 0.6) × 10^{-6}
		0.004	0.003			0.004	0.003	0.01	0.007							
	49	0.624 ± 0.065		(2.23 ± 0.05) × 10^{-4}	(1.64 ± 0.05) × 10^{-4}	0.622 ± 0.064		1.377 ± 0.693		(6.62 ± 0.04) × 10^{-4}	(4.9 ± 0.1) × 10^{-5}	0.510 ± 0.003	(1.06 ± 0.02) × 10^{-3}	(7.8 ± 0.2) × 10^{-5}	(1.72 ± 0.03) × 10^{-4}	(1.27 ± 0.02) × 10^{-5}
		0.006	0.002			0.006	0.002	0.008	0.004							
Gluconate	25	0.050 ± 0.202		(4.33 ± 0.1) × 10^{-3}	(1.585 ± 0.003) × 10^{-3}	0.0489 ± 0.001	0.200 ± 0.002	0.504 ± 0.006	0.256 ± 0.003	(1.283 ± 0.009) × 10^{-4}	(4.69 ± 0.02) × 10^{-4}	0.187 ± 0.002	(2.79 ± 0.09) × 10^{-4}	(1.02 ± 0.02) × 10^{-4}	(4.5 ± 0.1) × 10^{-6}	(1.64 ± 0.03) × 10^{-5}
		0.001	0.002													
	37	0.078 ± 0.289		(4.49 ± 0.1) × 10^{-4}	(1.407 ± 0.006) × 10^{-3}	0.077 ± 0.004	0.288 ± 0.007	0.77 ± 0.02	0.37 ± 0.01	(1.25 ± 0.02) × 10^{-4}	(3.92 ± 0.02) × 10^{-4}	0.268 ± 0.008	(6.1 ± 0.5) × 10^{-5}	(1.9 ± 0.1) × 10^{-4}	(9.0 ± 0.7) × 10^{-6}	(2.8 ± 0.1) × 10^{-5}
		0.004	0.007													
	49	0.113 ± 0.49		(3.76 ± 0.1) × 10^{-4}	(1.219 ± 0.003) × 10^{-4}	0.112 ± 0.004	0.49 ± 0.01	1.21 ± 0.03	0.61 ± 0.01	(1.07 ± 0.02) × 10^{-4}	(3.46 ± 0.02) × 10^{-4}	0.44 ± 0.01	(1.39 ± 0.08) × 10^{-4}	(4.5 ± 0.2) × 10^{-4}	(2.1 ± 0.1) × 10^{-5}	(6.8 ± 0.4) × 10^{-5}
		0.003	0.01													

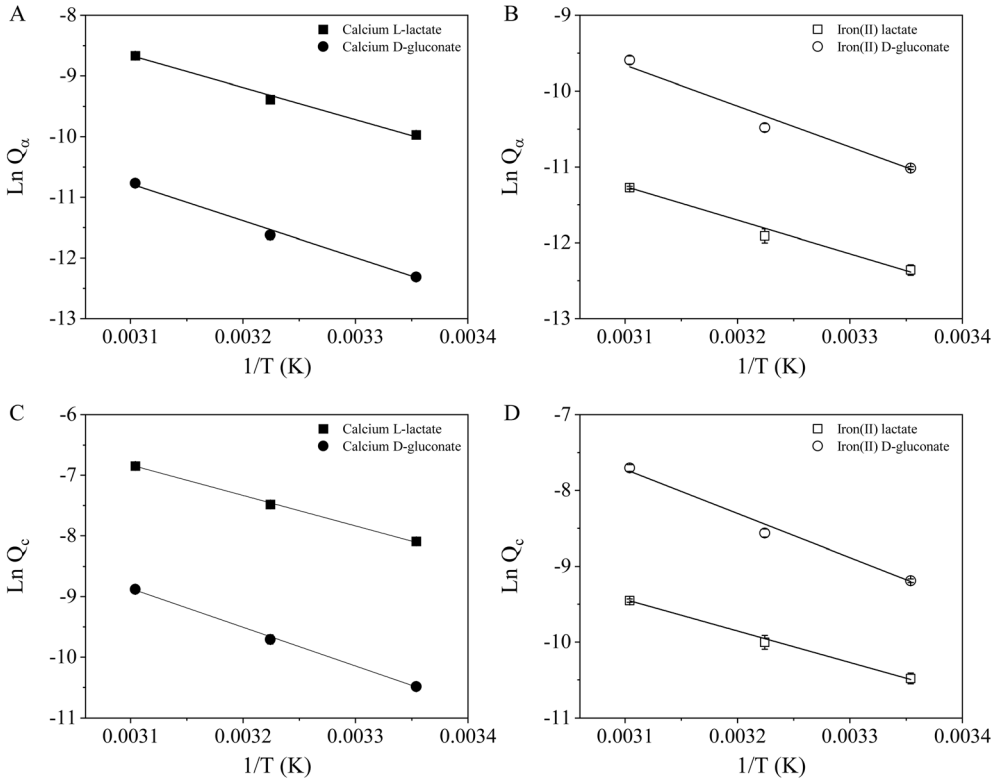

Fig. 4 Effect of temperature on the ionic products (Q_α and Q_c) of calcium and iron(II) hydroxycarboxylates in mixed solutions. Q_α (A and B) was calculated based on activity, while Q_c (C and D) was calculated based on concentration. The mixtures studied included calcium L-lactate and iron(II) lactate, as well as calcium D-gluconate and iron(II) D-gluconate.

$$FeLac^+ + Lac^- \rightarrow FeLac_2\downarrow \quad (22)$$

In accordance with Le Chatelier's principle, the equilibrium shifted towards solid $FeLac_2$ formation as lactate ion concentration increased. This resulted in a reduced soluble $FeLac_2$ fraction at equilibrium, with calcium L-lactate comprising approximately 87% of the composition in the saturated solution. The $\Delta H_{dis,\alpha}$ and $\Delta S_{dis,\alpha}$ values for calcium L-lactate in the mixed system were found to be remarkably similar to those of the pure calcium L-lactate solution. This suggested that the presence of iron(II) lactate did not significantly alter the dissolution thermodynamics of calcium L-lactate. In contrast, iron(II) lactate exhibited a substantial change in its thermodynamic parameters when in the mixed system. The $\Delta H_{dis,\alpha}$ increased from 13.51 ± 0.01 kJ mol^{-1} in the pure solution to 36 ± 2 kJ mol^{-1} in the mixed system, while the $\Delta S_{dis,\alpha}$ shifted from −60.0 ± 0.1 J mol^{-1} K^{-1} to 18 ± 5 J mol^{-1} K^{-1} (Table 2). This dramatic change indicated a significant alteration in the solvation environment of iron(II) ions in the presence of calcium lactate.

The $CaGlu_2$ + $FeGlu_2$ system exhibited similar behavior, albeit with a crucial difference. Calcium D-gluconate possessed lower solubility compared to iron(II) D-gluconate, making it more susceptible to precipitation:

$$CaGlu^+ + Glu^- \rightarrow CaGlu_2\downarrow \quad (23)$$

Consequently, iron(II) D-gluconate constituted about 80% of the composition in this saturated solution. Analysis of the solution components revealed that the ion activity ($\alpha_{Ca^{2+}}$ and $\alpha_{Fe^{2+}}$) in the mixed solutions were significantly reduced compared to their respective saturated single-salt solutions. In the $CaLac_2$ + $FeLac_2$ system, the ionic products $Q_{CaLac_2,\alpha}$and $Q_{FeLac_2,\alpha}$, based on activities, could be compared to their respective solubility products, $K_{sp,\alpha}$. The results presented in Table 3 demonstrated that the calculated ionic products were either larger than or close to the solubility products. This observation can be attributed to the increased total lactate or gluconate (T_{L^-}) concentration in the system, which effectively doubled due to the presence of both calcium and iron salts.[22] The $\Delta H_{dis,\alpha}$ and $\Delta S_{dis,\alpha}$ values for calcium D-gluconate increased in the mixed system. This suggested that the presence of iron(II) D-gluconate enhanced the endothermic nature of calcium D-gluconate dissolution and increased the disorder of the system. While thermodynamic parameters for iron(II) D-gluconate remain relatively stable in the mixed system. These findings clearly demonstrated that in homologous mixtures, the presence of a competing salt significantly altered the dissolution thermodynamics, with the effect being more pronounced for the less soluble salt (iron(II) lactate and calcium D-gluconate, respectively) in each system.

3.4.2 Cross-ligand interactions in mixed calcium lactate and iron(II) gluconate solutions. Previous studies have shown that sodium gluconate can induce the dissolution of calcium

lactate in an already saturated aqueous solution, driven by complex formation between calcium and gluconate.[38] This process can lead to the formation of supersaturated calcium gluconate in the homogeneous solution. We observed similar behavior when sodium gluconate was replaced with iron(II) gluconate. The iron(II) gluconate facilitated the dissolution of calcium lactate in a saturated aqueous solution. Notably, the time required for complete dissolution increased with higher amounts of iron(II) gluconate. A linear relationship was established between the critical mass of iron(II) gluconate required to completely dissolve a certain mass of calcium lactate. This relationship is described by the equation: [iron(II) gluconate] = 0.94 [calcium lactate] − 0.30. This linear correlation, as shown in Fig. 5A, indicated a strong interplay between these two salts in solution. Extrapolation of the linear curve to zero iron(II) gluconate concentration yields a calcium lactate concentration of 0.32 mol L^{-1}, indicating supersaturation (given that the measured solubility of calcium lactate is approximately 0.30 mol L^{-1}).

The analysis of the mixed solutions revealed two distinct behaviors, depending on the relative concentrations of calcium lactate and iron(II) gluconate. Calcium lactate supersaturated, iron(II) gluconate unsaturated, in this scenario, represented by white symbols in Fig. 5A, we observed the formation of a stable, homogeneous clarified solution. This condition maintained its clarity without precipitation over an extended period. When the concentration of iron(II) gluconate exceeded a critical threshold, resulting in both calcium lactate and iron(II) gluconate being supersaturated (indicated by gray symbols in Fig. 5A), we observed more complex behavior. It's worth noting that iron(II)

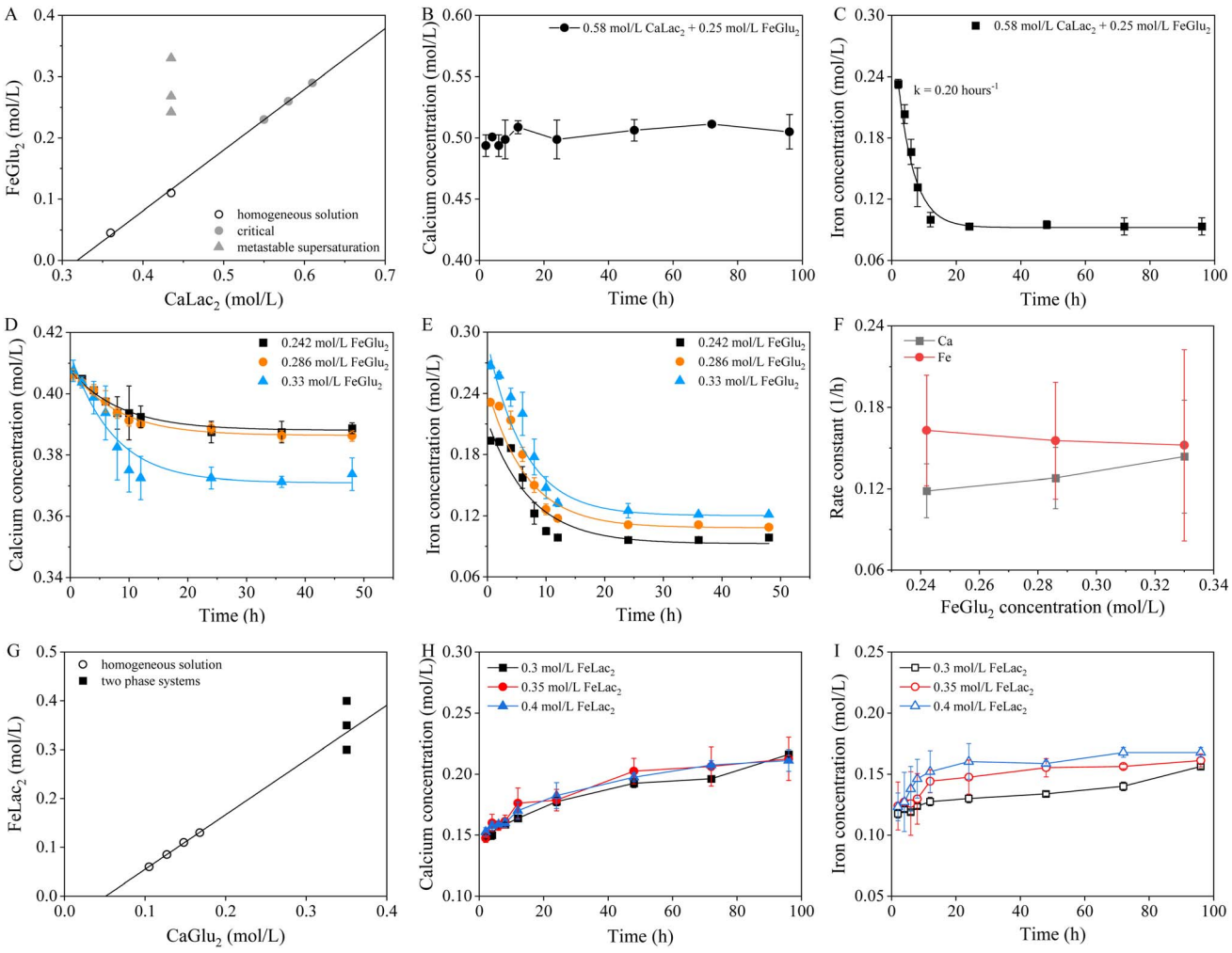

Fig. 5 Different combinations of calcium L-lactate and iron(II) D-gluconate in 100 mL of water (A), with grey symbols indicating metastable supersaturated solutions, and white circles representing samples that remained completely dissolved. Changes in total calcium concentration over time for a 0.58 mol per L calcium L-lactate and 0.25 mol per L iron(II) D-gluconate mixture (B). Changes in total iron(II) concentration over time for a 0.58 mol per L calcium L-lactate and 0.25 mol per L iron(II) D-gluconate mixture (C). Effect of adding different amounts of iron(II) D-gluconate on the final calcium concentration in the solution (D). Effect of adding different amounts of iron(II) D-gluconate on the final iron(II) concentration in the solution (E). First-order rate constants for precipitation determined by exponential fitting (F). Different combinations of calcium D-gluconate and iron(II) lactate in 100 mL of water (G), with black squares representing two-phase systems, and white circles denoting complete dissolution. Dissolved calcium concentration over time for different calcium D-gluconate and iron(II) lactate mixtures in two-phase systems (H). Dissolved iron concentration over time for different calcium D-gluconate and iron(II) lactate mixtures in two-phase systems (I).

gluconate has the highest solubility among the salts in the system containing calcium, iron, lactate, and gluconate ions. In this supersaturated state, initially, no immediate precipitation occurred, indicating a metastable condition. Precipitation eventually took place after a lag phase, which could last up to 2 hours, depending on the iron(II) gluconate concentration. This process was observed during constant stirring of the solution. The concentration of iron(II) gluconate significantly influenced both the clarification and precipitation periods. Higher iron(II) gluconate concentrations generally led to longer clarification times. Conversely, these higher concentrations tended to shorten the onset time of turbidity, indicating a faster initiation of the precipitation process. At iron(II) gluconate concentrations of 0.242 mol L^{-1} and 0.286 mol L^{-1} (with 0.435 mol per L calcium lactate), solutions showed similar clarification and precipitation times (approximately 15 minutes and 2.5 hours, respectively). Increasing iron(II) gluconate to 0.33 mol L^{-1} extended clarification time to 19 minutes but reduced precipitation time to 2 hours.

After 24 hours, the system reached an equilibrium state, as evidenced by stable concentrations of calcium and iron in solution. This is illustrated in Fig. 5B and C for the system containing the highest amount of calcium lactate (0.58 mol L^{-1}), which served as a representative example among the concentrations investigated. The concentration of iron in the filtered solution decreased more significantly, and the rate of iron precipitation could be described by a first-order reaction for the disappearance of iron in solution, with a half-life of approximately 3.46 hours (Fig. 5C). Notably, the equilibrium concentration of calcium decreased with increasing additions of iron(II) gluconate, suggesting a competitive interaction between the two metal ions for available ligands. The kinetics of this process followed a first-order reaction model for both calcium and iron concentration changes, as demonstrated in Fig. 5D and E. Interestingly, the pseudo-first-order rate constants for calcium increased linearly with increasing iron(II) gluconate concentration, while those for iron showed a decreasing trend under the same conditions (Fig. 5F).

To gain a better understanding of the mixed solutions, ion speciation was calculated based on the concentration-based association constant (K_c) shown in Table 1. In the mixed solution, four primary association reactions occur:

$$Ca^{2+} + Lac^- \rightleftharpoons CaLac^+ \quad K_c = \frac{[CaLac^+]}{[Ca^{2+}][Lac^-]} \tag{24}$$

$$Ca^{2+} + Glu^- \rightleftharpoons CaGlu^+ \quad K_c = \frac{[CaGlu^+]}{[Ca^{2+}][Glu^-]} \tag{25}$$

$$Fe^{2+} + Lac^- \rightleftharpoons FeLac^+ \quad K_c = \frac{[FeLac^+]}{[Fe^{2+}][Lac^-]} \tag{26}$$

$$Fe^{2+} + Glu^- \rightleftharpoons FeGlu^+ \quad K_c = \frac{[FeGlu^+]}{[Fe^{2+}][Glu^-]} \tag{27}$$

These reactions, along with three mass balance equations

Table 4 Total calcium/iron(II) concentration ($c_{Ca^{2+}}/c_{Fe^{2+}}$), speciation (calculated free calcium/iron(II) concentration ($[Ca^{2+}]/[Fe^{2+}]$), calculated calcium/iron(II) hydroxycarboxylates complex concentration ($[CaLac^+]$, $[CaGlu^+]$, $[FeLac^+]$, and $[FeGlu^+]$), calculated free hydroxycarboxylates concentration ($[Lac^-]/[Glu^-]$)), ionic strengths (I), ion activities ($\alpha_{Ca^{2+}}$, $\alpha_{Fe^{2+}}$, and α_{L^-}), and ionic products based on concentration (Q_c) for the dissolution of calcium lactate and iron(II) gluconate mixtures at 25 °C. Ionic concentrations are considered to remain constant when the solution is completely clarified. Data are expressed as mean ± SD from three independent experiments and three replicates

Added calcium L-lactate (mol L^{-1})	Added iron(II) D-gluconate (mol L^{-1})	$c_{Ca^{2+}}$	$c_{Fe^{2+}}$	$[Ca^{2+}]$	$[Lac^-]$	$[CaLac^+]$	$[Glu^-]$	$[CaGlu^+]$	$[Fe^{2+}]$	$[FeLac^+]$	$[FeGlu^+]$	Q_{CaLac_2}	Q_{CaGlu_2}	Q_{FeLac_2}	Q_{FeGlu_2}
0.36	0.045	0.36	0.045	0.00258	0.368	0.311	0.039	0.046	0.00023	0.040	0.00450	3.51×10^{-4}	4.01×10^{-6}	3.12×10^{-5}	3.57×10^{-7}
0.435	0.11	0.435	0.11	0.00226	0.449	0.332	0.098	0.101	0.000418	0.089	0.0204	4.56×10^{-4}	2.20×10^{-5}	8.43×10^{-5}	4.06×10^{-6}
0.58	0.251	0.505 ± 0.007	0.093 ± 0.004	(2.43 ± 0.01) × 10^{-3}	0.518 ± 0.007	0.412 ± 0.004	0.082 ± 0.003	0.090 ± 0.003	(3.21 ± 0.07) × 10^{-4}	0.079 ± 0.003	0.0131 ± 0.0008	(6.5 ± 0.2) × 10^{-4}	(1.6 ± 0.1) × 10^{-5}	(8.6 ± 0.4) × 10^{-5}	(2.2 ± 0.2) × 10^{-6}
0.435	0.242	0.389 ± 0.002	0.099 ± 0.002	(2.25 ± 0.08) × 10^{-3}	0.402 ± 0.002	0.2960 ± 0.0004	0.089 ± 0.002	0.090 ± 0.001	(4.19 ± 0.04) × 10^{-4}	0.080 ± 0.001	0.0184 ± 0.0005	(3.64 ± 0.02) × 10^{-4}	(1.77 ± 0.06) × 10^{-5}	(6.8 ± 0.1) × 10^{-5}	(3.3 ± 0.2) × 10^{-6}
0.435	0.286	0.386 ± 0.002	0.109 ± 0.002	(2.19 ± 0.07) × 10^{-3}	0.400 ± 0.002	0.2867 ± 0.005	0.098 ± 0.002	0.097 ± 0.001	(4.54 ± 0.04) × 10^{-4}	0.086 ± 0.001	0.0221 ± 0.0006	(3.50 ± 0.02) × 10^{-4}	(2.11 ± 0.06) × 10^{-5}	(7.3 ± 0.1) × 10^{-5}	(4.4 ± 0.2) × 10^{-6}
0.435	0.33	0.374 ± 0.005	0.121 ± 0.002	(2.10 ± 0.02) × 10^{-3}	0.388 ± 0.005	0.267 ± 0.006	0.110 ± 0.002	0.1049 ± 0.0007	(5.1 ± 0.1) × 10^{-4}	0.0931 ± 0.0007	0.028 ± 0.001	(3.2 ± 0.1) × 10^{-4}	(2.55 ± 0.06) × 10^{-5}	(7.60 ± 0.04) × 10^{-5}	(6.1 ± 0.3) × 10^{-6}

$$[Ca^{2+}] + [CaLac^{+}] + [CaGlu^{+}] = c_{Ca^{2+}} \quad (28)$$

$$[Fe^{2+}] + [FeLac^{+}] + [FeGlu^{+}] = c_{Fe^{2+}} \quad (29)$$

$$[CaLac^{+}] + [FeLac^{+}] + [Lac^{-}] = 2c_{Ca^{2+}} \quad (30)$$

and an equation for electroneutrality,

$$2[Ca^{2+}] + 2[Fe^{2+}] + [CaLac^{+}] + [FeLac^{+}] + [CaGlu^{+}] + [FeGlu^{+}] = [Lac^{-}] + [Glu^{-}] \quad (31)$$

Eight unknowns were determined for each experiment using nonlinear optimization techniques. The equilibrium concentrations for each experiment are presented in Table 4. Speciation analysis of the mixed solutions revealed that the free ion concentrations ($[Ca^{2+}]$ and $[Fe^{2+}]$) were substantially lower than the total metal concentrations, indicating significant complex formation. The dominant species in solution were the metal–ligand complexes ($[CaLac^{+}]$, $[FeLac^{+}]$, $[CaGlu^{+}]$, and $[FeGlu^{+}]$). As the iron(II) gluconate concentration increased, a general trend of decreasing $[Ca^{2+}]$ and increasing $[Fe^{2+}]$ was observed, further supporting the competitive nature of the metal–ligand interactions.

Moreover, the ionic products (Q) for calcium gluconate and lactate were compared with their respective solubility products. For calcium gluconate, $[Ca^{2+}][Glu^{-}]^2$ was compared with the solubility product of 1.57×10^{-5}, while for calcium lactate, $[Ca^{2+}][Lac^{-}]^2$ was compared with the solubility product of 2.75×10^{-4}. The results indicated significant supersaturation, particularly for calcium lactate. This high concentration of calcium lactate is a result of the dissolution process in which the ionic product becomes larger than the solubility product during the dissolution of calcium lactate in iron(II) gluconate. This observation aligns with our previous results, which indicated that the presence of iron(II) could facilitate the dissolution of calcium salts (Fig. 3). Regarding iron salts, the filtered solution was supersaturated with iron(II) lactate when comparing the ionic products to the solubility products. This occurred because the dissociated calcium from calcium lactate has a higher K_c with Glu^{-}, resulting in more Lac^{-} being freed. Interestingly, iron(II) D-gluconate was not saturated due to the precipitation of iron and the binding of gluconate to calcium. This phenomenon can be attributed to ion exchange and competitive binding induction, as shown in eqn (32). The primary dissolution reaction, enhanced by the presence of gluconate, is described as:

$$CaLac^{+} + FeGlu^{+} \rightarrow CaGlu^{+} + FeLac^{+}$$
$$K_1 = \frac{[CaGlu^{+}][FeLac^{+}]}{[CaLac^{+}][FeGlu^{+}]} = 1.35 \pm 0.02 \quad (32)$$

The equilibrium constant (K_1) for this reaction is 1.35, indicating that the equilibria shift forward. Consequently, $CaLac^{+}$ was converted to $CaGlu^{+}$, and similarly, Fe^{2+} showed a tendency to bind with Lac^{-} compared to Ca^{2+}. The reaction

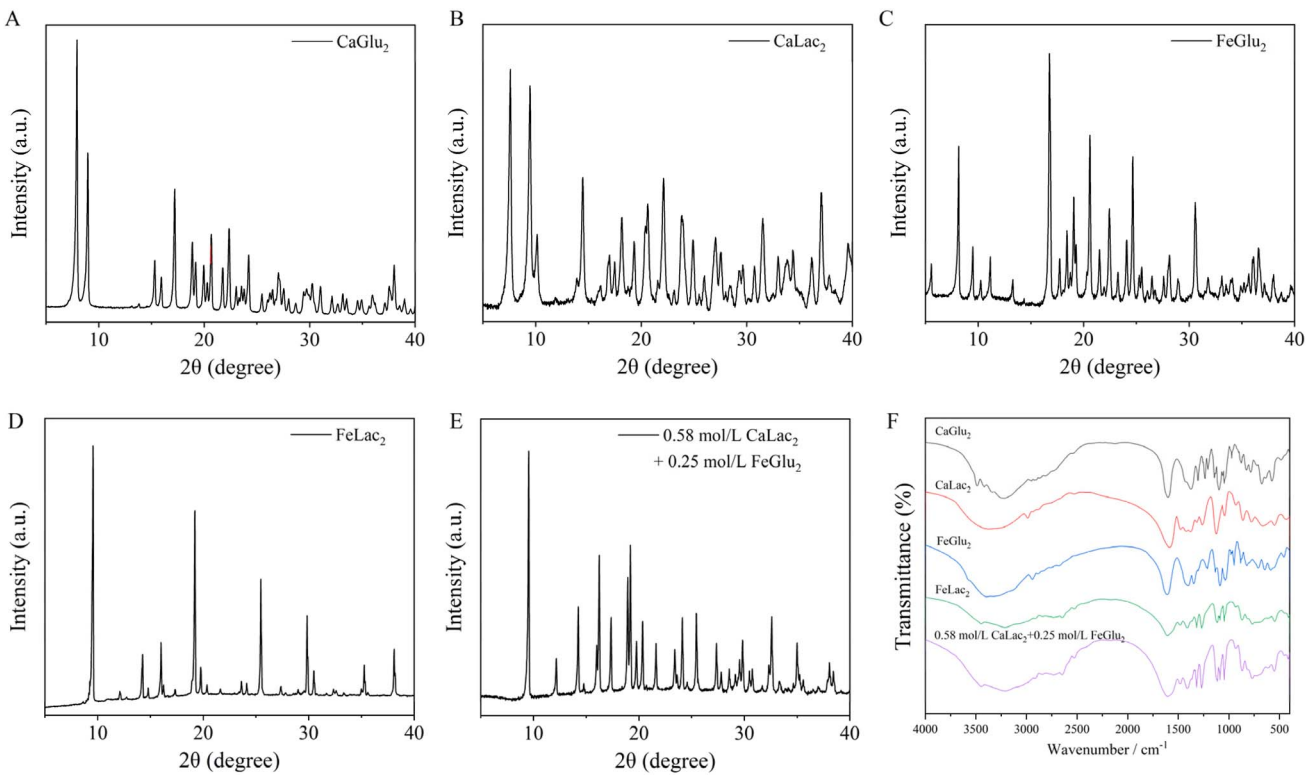

Fig. 6 X-ray diffractograms of calcium D-gluconate monohydrate (A), calcium L-lactate pentahydrate (B), iron(II) D-gluconate dihydrate (C), iron(II) lactate (D), and the precipitate formed from a 0.58 mol per L calcium L-lactate and 0.25 mol per L iron(II) D-gluconate mixture solution after 96 hours of equilibration (E). Fourier transform infrared (FTIR) spectra of the same samples (F).

described in eqn (31) was constrained by the ligand–metal ion exchange occurring within a closed system. To further understand the precipitation dynamics, we analyzed the ionic products (Q) for various potential precipitates ($CaGlu_2$, $FeLac_2$, and $FeGlu_2$), which provided valuable insights into the thermodynamic driving forces for precipitation. Consistently, Q_{FeLac_2} exhibited the highest values among the analyzed compounds, explaining the preferential precipitation of iron(II) lactate. Furthermore, all Q values showed an increasing trend with rising iron(II) gluconate concentrations, indicating a higher degree of supersaturation under these conditions. This observation aligns with the fact that $FeLac_2$ has the lowest solubility product (K_{sp}) among the four salts in the system, making it the most likely to precipitate as iron(II) lactate. To confirm the identity of the precipitate, we conducted X-ray diffractometry and FT-IR spectroscopy analyses.[39] As illustrated in Fig. 6, these comparative analyses conclusively identified the precipitate as iron(II) lactate.

Furthermore, above observations can be rationalized by considering several interacting factors. The presence of multiple ligands (lactate and gluconate) and metal ions (Ca^{2+} and Fe^{2+}) established a complex equilibrium involving various metal–ligand complexes. This cross-ligand complexation enhanced the overall solubility of the system, outweighing the common ion effect that would typically decrease calcium gluconate solubility upon the addition of iron(II) gluconate. The initial formation of metastable, supersaturated solutions can be attributed to kinetic factors, with the lag time before precipitation representing the period required for nucleation and crystal growth to overcome energy barriers. The complex dependence of clarification and precipitation times on iron(II) gluconate concentration suggested a delicate balance between supersaturation (the thermodynamic driving force) and the kinetics of nucleation and crystal growth. As iron(II) lactate precipitated, it removed both iron(II) and lactate ions from solution, shifting the equilibrium and leading to the observed changes in speciation and the continued dissolution of calcium lactate. The decreasing trend in calcium concentration with increasing iron(II) gluconate suggested that iron competed effectively for the ligands, potentially forming stronger complexes than calcium.

The first-order kinetics for changes in calcium and iron concentrations imply that the rate-limiting step involves desolvation or rearrangement of metal–ligand complexes, rather than nucleation or crystal growth itself. The contrasting trends in rate constants (increasing for calcium, decreasing for iron) with increasing iron(II) gluconate concentration suggest a complex interplay between thermodynamic driving forces and kinetic factors. Higher iron concentrations may accelerate initial iron(II) lactate precipitation, increasing the rate of calcium concentration change. However, this rapid precipitation may form a protective layer or increase viscosity, slowing subsequent iron precipitation and explaining its declining rate constant.

3.4.3 Cross-ligand interactions in mixed calcium gluconate and iron(II) lactate solutions. The reverse experiment, involving the addition of calcium gluconate and iron(II) lactate to an aqueous solution, exhibited markedly different dissolution behavior compared to the previous system. As the concentrations of these salts increased, the time required for the formation of a clarified solution was progressively prolonged. For instance, when 0.168 mol per L $CaGlu_2$ and 0.13 mol per L $FeLac_2$ were added, the clarification process extended beyond 12 hours, indicating a significantly slower dissolution process in this system. Further increases in the concentration of calcium and iron salts resulted in the formation of two-phase systems, with no additional clarified solutions observed. Based on these observations, the dissolution process could be categorized into two types: clarified and non-clarified, as illustrated in Fig. 5G. It was noteworthy that homogeneous solutions did not form when calcium gluconate and iron(II) lactate concentrations reached 0.35 mol L^{-1} and 0.30 mol L^{-1} or higher, respectively. In the two-phase systems, calcium gluconate and iron(II) lactate only partially dissolved, with increases in total calcium/iron concentration attributed to complex formation. We monitored the concentrations of calcium and iron during the dissolution process, as depicted in Fig. 5H and I. When the concentration of iron(II) lactate ranged from 0.3 to 0.4 mol L^{-1}, the solubility of calcium gluconate demonstrated an increasing trend over time. After 96 hours of dissolution, the filtered concentration of calcium reached 0.2 mol L^{-1}. Similarly, the solubility of iron(II) lactate also increased, stabilizing at approximately 0.16 mol L^{-1} after 96 hours. To gain deeper insights into the system's behavior, we also performed ion speciation analysis using non-linear optimization techniques. The results, presented in Table 5, revealed that the concentrations of [$CaLac^+$], [$CaGlu^+$], and [$FeLac^+$] were comparable, while [$FeGlu^+$] was slightly lower. This finding suggested that ion exchange between $CaGlu_2$ and $FeLac_2$ occurred during the dissolution process. However, it became evident that this was a slow, step-by-step ion-competitive binding reaction. As shown in eqn (33), $CaGlu^+$ and $FeLac^+$ may not undergo a fast direct ion exchange process due to the equilibrium constant K_2 being less than 1 and the dissolution kinetic evidence (prolonged equilibration and time-dependent solubility increases):

$$CaGlu^+ + FeLac^+ \rightarrow FeGlu^+ + CaLac^+$$
$$K_2 = \frac{[CaLac^+][FeGlu^+]}{[CaGlu^+][FeLac^+]} = 0.75 \pm 0.02 \quad (33)$$

Specifically, the reciprocal relationship $K_1 = 1/K_2$ holds within experimental error, validating our thermodynamic analysis. Furthermore, the analysis revealed that [$CaGlu^+$] and [$FeLac^+$] were generally higher than [$CaLac^+$] and [$FeGlu^+$], respectively, which was consistent with the lower equilibrium constant ($K_2 = 0.75$) for the exchange reaction (33). This indicated the absence of a strong driving force for direct exchange. Instead of a single, rapid exchange, this system underwent a slower, three-step process:

$$CaGlu^+ + Fe^{2+} \rightarrow FeGlu^+ + Ca^{2+} \ (K_3 = 1.10) \quad (34)$$

$$FeLac^+ + Glu^- \rightarrow FeGlu^+ + Lac^- \ (K_4 = 1.05) \quad (35)$$

Table 5 Total calcium/iron(II) concentration ($c_{Ca^{2+}}/c_{Fe^{2+}}$), speciation (calculated free calcium/iron(II) concentration ($[Ca^{2+}]/[Fe^{2+}]$), calculated calcium/iron(II) hydroxycarboxylates complex concentration ($[CaLac^+]$, $[CaGlu^+]$, $[FeLac^+]$, and $[FeGlu^+]$), calculated free hydroxycarboxylates concentration ($[Lac^-]/[Glu^-]$)), ionic strengths (I), ion activities ($\alpha_{Ca^{2+}}$, $\alpha_{Fe^{2+}}$, and α_{L^-}), and ionic products based on concentration (Q_c) for the dissolution of calcium gluconate and iron(II) lactate mixtures at 25 °C. Ionic concentrations are considered to remain constant when the solution is completely clarified. Data are expressed as mean ± SD from three independent experiments and three replicates

Added calcium D-gluconate (mol L^{-1})	Added iron(II) lactate (mol L^{-1})	$c_{Ca^{2+}}$	$c_{Fe^{2+}}$	$[Ca^{2+}]$	$[Lac^-]$	$[CaLac^+]$	$[Glu^-]$	$[CaGlu^+]$	$[Fe^{2+}]$	$[FeLac^+]$	$[FeGlu^+]$	Q_{CaLac_2}	Q_{CaGlu_2}	Q_{FeLac_2}	Q_{FeGlu_2}
0.105	0.06	0.105	0.06	0.0017	0.1108	0.06053	0.0566	0.04279	7.34×10^{-4}	0.03863	0.02063	2.05×10^{-5}	5.34×10^{-6}	9.01×10^{-6}	2.35×10^{-6}
0.127	0.085	0.127	0.085	0.00156	0.1339	0.06844	0.0805	0.05699	8.13×10^{-4}	0.05168	0.03251	2.80×10^{-5}	1.01×10^{-5}	1.46×10^{-5}	5.26×10^{-6}
0.148	0.11	0.148	0.11	0.00149	0.1559	0.07597	0.1045	0.07054	8.66×10^{-4}	0.06415	0.04499	3.62×10^{-5}	1.63×10^{-5}	2.11×10^{-5}	9.46×10^{-6}
0.168	0.1317	0.168	0.1317	0.00145	0.1768	0.08406	0.1252	0.08248	8.95×10^{-4}	0.07513	0.05568	4.55×10^{-5}	2.28×10^{-5}	2.80×10^{-5}	1.40×10^{-5}
0.35	0.3	0.216 ± 0.002	0.156 ± 0.002	(1.52 ± 0.01) × 10^{-3}	0.227 ± 0.002	0.113 ± 0.002	0.148 ± 0.002	0.1018 ± 0.0003	(8.57 ± 0.09) × 10^{-4}	0.0924 ± 0.0003	0.063 ± 0.001	(7.8 ± 0.2) × 10^{-5}	(3.32 ± 0.05) × 10^{-5}	(4.42 ± 0.02) × 10^{-5}	(1.87 ± 0.07) × 10^{-5}
0.35	0.35	0.21 ± 0.02	0.161 ± 0.005	(1.5 ± 0.1) × 10^{-3}	0.22 ± 0.03	0.10 ± 0.02	0.153 ± 0.006	0.101 ± 0.004	(9.0 ± 0.7) × 10^{-4}	0.092 ± 0.003	0.068 ± 0.008	(7 ± 2) × 10^{-5}	(3.419 ± 0.003) × 10^{-5}	(4.2 ± 0.6) × 10^{-5}	(2.1 ± 0.3) × 10^{-5}
0.35	0.4	0.211 ± 0.009	0.168 ± 0.004	(1.45 ± 0.01) × 10^{-3}	0.222 ± 0.009	0.105 ± 0.005	0.159 ± 0.003	0.105 ± 0.003	(9.04 ± 0.09) × 10^{-4}	0.095 ± 0.003	0.0716 ± 0.0009	(7.1 ± 0.7) × 10^{-5}	(3.7 ± 0.2) × 10^{-5}	(2.3 ± 0.3) × 10^{-5}	(2.3 ± 0.8) × 10^{-5}

$$Ca^{2+} + Lac^- \rightarrow CaLac^+ \ (K_c > 1) \quad (36)$$

This stepwise mechanism allowed the system to navigate around the unfavorable direct exchange while still ultimately moving towards a thermodynamically preferred state. The slower kinetics indicated that as ions were exchanged, they had sufficient time to reach their solubility limits and precipitate, thereby preventing the formation of a fully supersaturated solution. At higher concentrations, this mixture formed a two-phase system rather than a homogeneous solution, suggesting that precipitation occurred before a supersaturated state could be achieved. Comparing this system to the calcium lactate and iron(II) gluconate mixture, we observed that the current mixture did not form a stable solution because both calcium gluconate and iron(II) lactate were at or near their solubility limits. Calcium gluconate, having a much lower solubility compared to calcium lactate, was more prone to precipitation. Moreover, there was no excess of either lactate or gluconate ions to promote the solubility of the other metal ion. The lower solubilities of both salts and the lack of a highly soluble component led to instability and potential precipitation. Furthermore, the key distinction between the two systems lies in the kinetics and thermodynamics of the ion exchange processes. The rapid, favorable exchange in the calcium lactate and iron(II) gluconate system allowed it to reach a metastable supersaturated state before precipitation occurred. In contrast, the slower, stepwise process in the calcium gluconate and iron(II) lactate system allowed precipitation to occur concurrently with dissolution and ion exchange, preventing the formation of a fully supersaturated solution. This provided a consistent explanation for our observations of longer clarification times and the formation of two-phase systems at higher concentrations in the calcium gluconate and iron(II) lactate mixture.

3.5 Isothermal titration calorimetry

The investigation of ion exchange processes in mixed metal–ligand solutions revealed intricate thermodynamic and kinetic behaviors governing the formation of supersaturated solutions and subsequent precipitation. Isothermal titration calorimetry (ITC) data, as shown in Fig. 7 and Table 6, provided crucial insights into the thermodynamic parameters driving these interactions. The results demonstrated that all observed reactions in both systems ($CaLac_2$ + $FeGlu_2$ and $CaGlu_2$ + $FeLac_2$) were spontaneous, as evidenced by negative Gibbs free energy (ΔG) values ranging from −19.19 to −20.61 kJ mol^{-1}. This narrow range suggested comparable overall energetics across all reactions, regardless of direction or specific ions involved. The exothermic nature of these reactions (Fig. 7), indicated by negative enthalpy (ΔH) values (Table 6), implied the formation of more stable complexes during the ion exchange process. Furthermore, the positive entropy (ΔS) values observed in all cases pointed to an increase in disorder, likely due to the disruption of hydration shells surrounding the ions during exchange.[40]

As can be seen from Table 6, in the $CaLac_2$ + $FeGlu_2$ system, the ion exchange process appeared to be more straightforward.

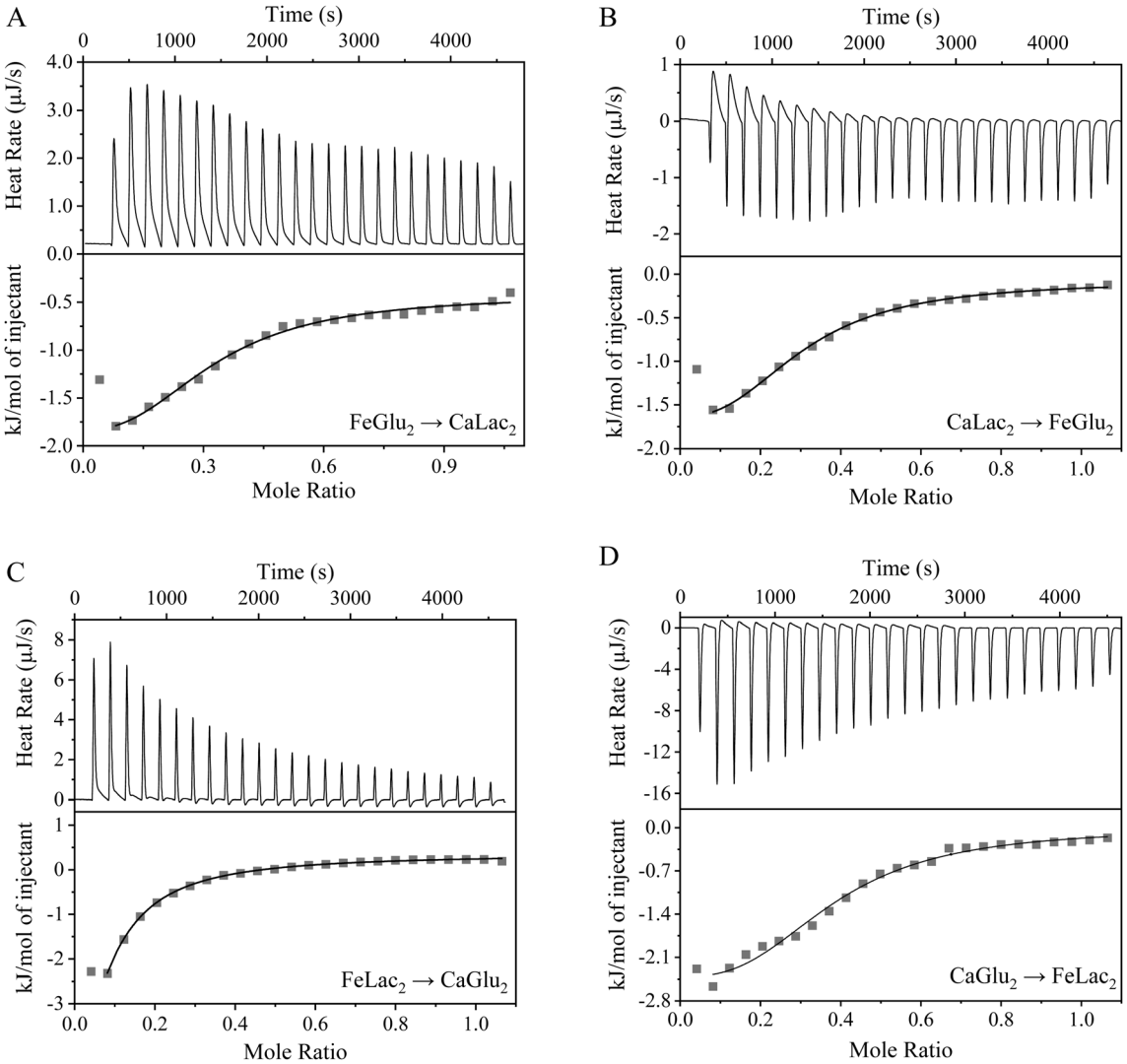

Fig. 7 Isothermal titration calorimetry (ITC) isotherms illustrating the heat effects of reactions measured in the titration of iron(II) D-gluconate into calcium L-lactate (A), calcium L-lactate into iron(II) D-gluconate (B), iron(II) lactate into calcium D-gluconate (C), and calcium D-gluconate into iron(II) lactate (D) in MES buffer at pH 5.0 and 25 °C. Solid lines are the one-type-of-site model fitting.

The apparent association constant (K_A) for the forward ($FeGlu_2 \rightarrow CaLac_2$, $K_A = 2383 \pm 142$) and reverse ($CaLac_2 \rightarrow FeGlu_2$, $K_A = 2315 \pm 386$) reactions indicated a relatively balanced exchange. This balance facilitated rapid ion exchange, leading to the more readily observed formation of supersaturated solutions in this system. Conversely, the $CaGlu_2$ + $FeLac_2$ system exhibited more complex behavior. As mentioned before, the direct exchange reaction (34) was not spontaneous, with an equilibrium constant $K_2 < 1$ (0.75). However, the ITC data revealed a higher association constant for the overall process ($CaGlu_2 \rightarrow FeLac_2$, $K_A = 4185 \pm 942$) compared to its reverse reaction ($FeLac_2 \rightarrow CaGlu_2$, $K_A = 2587 \pm 25$). This apparent contradiction was reconciled by considering a step-wise exchange mechanism shown in reactions eqn (34)–(36). Each step in this process could be thermodynamically favorable ($K > 1$) even if the direct exchange was not. This step-wise mechanism allowed the system to navigate around the energy barrier of the direct exchange through a series of more favorable intermediate steps, ultimately reaching a more stable final state as indicated by the higher overall K_A.[41] Furthermore, the slightly higher K_A for the $CaGlu_2 \rightarrow FeLac_2$ reaction corroborated the need for a step-wise process in that mixture. This step-wise mechanism inherently resulted in slower kinetics compared to a direct exchange. Moreover, kinetic factors could influence the ITC results, especially if the system didn't reach full equilibrium during the measurement time. The direction of titration ($CaGlu_2 \rightarrow FeLac_2$ *vs.* $FeLac_2 \rightarrow CaGlu_2$) may interact differently with these slower kinetics, potentially affecting the extent to which equilibrium was reached during measurement. This interplay between the step-wise process, slower kinetics, and titration direction could ultimately lead to the observed differences in overall association constants between the forward and reverse reactions. The differences in behavior between the two systems could thus be attributed to the thermodynamics

Table 6 Thermodynamic parameters (ΔH, ΔS, ΔG, and apparent association constant K_A) for the titrations of iron(II) D-gluconate into calcium L-lactate, calcium L-lactate into iron(II) D-gluconate, iron(II) lactate into calcium D-gluconate, and calcium D-gluconate into iron(II) lactate at pH 5.0 and 25 °C. Data are expressed as mean ± SD from three independent experiments and three replicates[a]

Titration	ΔH (kJ mol^{-1})	ΔS (J mol^{-1} K^{-1})	$-T\Delta S$ (kJ mol^{-1})	ΔG (kJ mol^{-1})	K_A
$FeGlu_2 \rightarrow CaLac_2$	-1.835 ± 0.381^a	58.34 ± 0.72^a	-17.39 ± 0.22^a	-19.27 ± 0.15^a	2383 ± 142^a
$CaLac_2 \rightarrow FeGlu_2$	-2.086 ± 0.191^a	56.89 ± 2.19^a	-16.94 ± 0.65^a	-19.19 ± 0.89^a	2315 ± 386^a
$FeLac_2 \rightarrow CaGlu_2$	-6.435 ± 0.298^b	43.65 ± 0.15^b	-13.01 ± 0.05^b	-19.47 ± 0.02^a	2587 ± 25^a
$CaGlu_2 \rightarrow FeLac_2$	-2.875 ± 0.467^c	60.25 ± 3.78^a	-17.96 ± 1.12^a	-20.61 ± 0.80^a	4185 ± 942^b

[a] Values in the same column with different superscript letters were significantly different (ANOVA followed by Tukey's test, $p < 0.05$).

and kinetics of their respective ion exchange processes. These factors contributed to the observed differences in dissolution rates, supersaturation behavior, and precipitation kinetics between the two systems.[42]

4. Conclusion

This comprehensive study on calcium and iron(II) hydroxycarboxylates revealed critical insights into their aqueous behavior and interactions, with significant implications for mineral supplementation and food fortification. Our findings demonstrated unexpected solubility trends, with calcium lactate and iron(II) gluconate exhibiting higher solubilities than their counterparts due to the complex interplay between metal ion properties (size, charge density), ligand characteristics (size, coordination ability), and the resulting crystal structure properties (packing efficiency, intermolecular forces). The observed enhancement of calcium solubility in the presence of iron(II) ions suggested potential synergistic effects in mixed mineral formulations. Analysis of homologous and cross-ligand systems uncovered complex speciation patterns and step-wise ion exchange processes, particularly in the calcium lactate and iron(II) gluconate mixture, which formed metastable supersaturated solutions. These thermodynamic and kinetic insights, corroborated by isothermal titration calorimetry, provided a robust scientific foundation for optimizing mineral delivery systems. By elucidating the intricate interplay between these essential minerals, our research offers valuable guidance for developing more effective and bioavailable mineral supplements, potentially providing strategies to combat global mineral deficiencies and enhance human nutrition.

Author contributions

Yi Li: conceptualization, data curation, formal analysis, investigation, methodology, validation, visualization, writing – original draft. Yongqiang Cheng: resources, supervision, funding acquisition. Ning Tang: conceptualization, methodology, funding acquisition, project administration, supervision, writing – review & editing.

Conflicts of interest

There are no conflicts of interest to declare.

Data availability

The authors declare that the data supporting the findings of this study are included within the article.

Supplementary information: detailed methods for solubility determination, electrical conductivity measurements, density functional theory calculations, the preparation of mixed calcium hydroxycarboxylates and iron(II) chloride solutions, mixed calcium and iron(II) hydroxycarboxylates solutions, EDTA titration, $KMnO_4$ titration, X-ray diffraction, Fourier transform infrared spectroscopy, and isothermal titration calorimetry. See DOI: **https://doi.org/10.1039/d5ra04858c**.

Acknowledgements

This work was supported by National Natural Science Foundation of China (32001687).

References

1 L. L. Brown, B. E. Cohen, E. Edwards, C. E. Gustin and Z. Noreen, *J. Women's Health*, 2021, **30**, 207–211.
2 R. Olson, B. Gavin-Smith, C. Ferraboschi and K. Kraemer, *Nutrients*, 2021, **13**, 1118.
3 S. J. Fairweather-Tait and B. Teucher, *Nutr. Rev.*, 2002, **60**, 360–367.
4 D. A. Straub, *Nutr. Clin. Pract.*, 2007, **22**, 286–296.
5 B. Sandström, *Br. J. Nutr.*, 2001, **85**(Suppl 2), S181–S185.
6 Y. Li, Y. Q. Cheng and N. Tang, *Food Sci.*, 2024, **45**, 323–335.
7 F. D. Lorenzo, A. Burgos-Cara, E. Ruiz-Agudo, C. V. Putnis and M. Prieto, *CrystEngComm*, 2017, **19**, 447–460.
8 H. A. A. Alsaiari, A. Kan and M. B. B. Tomson, *SPE J.*, 2010, **15**, 294–300.
9 E. Alsubhe, A. D. Anastasiou, M. Mehrabi, E. M. Raif, A. Hassanpour, P. Giannoudis and A. Jha, *Mater. Sci. Eng., C*, 2020, **115**, 111053.
10 A. C. B. Delbem, K. M. R. P. Alves, K. T. Sassaki and J. C. S. Moraes, *Caries Res.*, 2012, **46**, 481–487.
11 T. Bechtold, E. Burtscher and A. Turcanu, *J. Chem. Soc., Dalton Trans.*, 2002, 2683–2688.
12 A. I. Abioye, T. A. Okuneye, A.-M. O. Odesanya, O. Adisa, A. I. Abioye, A. I. Soipe, K. A. Ismail, J. F. Yang, L.-K. Fasehun and M. O. Omotayo, *J. Nutr.*, 2021, **151**, 1084–1101.
13 M. Vavrusova, M. B. Munk and L. H. Skibsted, *J. Agric. Food Chem.*, 2013, **61**, 8207–8214.
14 A. C. Garcia, M. Vavrusova and L. H. Skibsted, *J. Agric. Food Chem.*, 2016, **64**, 2352–2360.
15 N. Tang and L. H. Skibsted, *J. Agric. Food Chem.*, 2017, **65**, 8727–8743.
16 J. Liu, N. Tang and Y. Cheng, *ACS Food Sci. Technol.*, 2023, **3**, 499–513.
17 M. Vavrusova, R. Liang and L. H. Skibsted, *J. Agric. Food Chem.*, 2014, **62**, 5675–5681.
18 M. Vavrusova, A. C. Garcia, B. P. Danielsen and L. H. Skibsted, *RSC Adv.*, 2017, **7**, 3078–3088.
19 M. Vavrusova, B. P. Danielsen, A. C. Garcia and L. H. Skibsted, *J. Food Drug Anal.*, 2018, **26**, 330–336.
20 C.-Q. Xiao, Q. Huang, Y. Zhang, H.-Q. Zhang and L. Lai, *Thermochim. Acta*, 2020, **691**, 178721.
21 A. Mishelevich and A. Apelblat, *J. Chem. Thermodyn.*, 2008, **40**, 897–900.
22 N. Kubantseva, R. W. Hartel and P. A. Swearingen, *J. Dairy Sci.*, 2004, **87**, 863–867.
23 N. Veiga, I. Macho, K. Gómez, G. González, C. Kremer and J. Torres, *J. Mol. Struct.*, 2015, **1098**, 55–65.
24 C. A. Johnson and J. A. Thomas, *J. Pharm. Pharmacol.*, 2011, **6**, 1037–1047.
25 A. Apelblat, E. Manzurola, J. Van Krieken and G. L. Nanninga, *Fluid Phase Equilib.*, 2005, **236**, 162–168.
26 L. H. Skibsted and G. Kilde, *Dan. Tidsskr. Farm.*, 1972, **46**, 41–46.
27 R. Shi, A. J. Cooper and H. Tanaka, *Nat. Commun.*, 2023, **14**, 4616.
28 P. Zheng, R. Zubatyuk, W. Wu, O. Isayev and P. O. Dral, *Nat. Commun.*, 2021, **12**, 7022.
29 X. Liu, H. Wang, W. Qiu, Q. Wu, H. Wang and S. Xue, *Sol. Energy*, 2022, **231**, 897–907.
30 A. Nimmermark, L. Öhrström and J. Reedijk, *Z. Kristallogr. – Cryst. Mater.*, 2013, **228**, 311–317.
31 M. Vavrusova, M. B. Munk and L. H. Skibsted, *J. Agric. Food Chem.*, 2013, **61**, 8207–8214.
32 X.-C. Liu and L. H. Skibsted, *Food Chem.*, 2022, **367**, 130674.
33 R. E. Herzog, Q. Shi, J. N. Patil and J. L. Katz, *Langmuir*, 1989, **5**, 861–867.
34 B. Shkembi and T. Huppertz, *Nutrients*, 2021, **14**, 180.
35 Y. Li, Y. Cheng and N. Tang, *Food Rev. Int.*, 2025, **41**, 345–372.
36 M. Vavrusova and L. H. Skibsted, *LWT–Food Sci. Technol.*, 2014, **59**, 1198–1204.
37 Y. Li, Y. Cheng and N. Tang, *Food Res. Int.*, 2025, **217**, 116853.
38 A. C. Garcia, J. S. Hansen, N. Bailey and L. H. Skibsted, *Food Res. Int.*, 2020, **137**, 109539.
39 V. Nikolic, D. Ilic, L. Nikolic, L. Stanojevic, M. Cakic, A. Tacic and S. Ilic-Stojanovic, *The synthesis and characterization of iron(II): Gluconate*, Savremene tehnologije, 2014, vol. 3, pp. 16–24.
40 D. Pyreu and M. Bazanova, *Inorg. Chim. Acta*, 2016, **453**, 687–691.
41 R. Yang, J. Tao, Q. Huang, B. Tie, M. Lei, Y. Yang and H. Du, *J. Soils Sediments*, 2019, **19**, 1319–1327.
42 B. K. Paul, *Chem. Phys. Impact*, 2022, **5**, 100104.